RSC Advances

This article can be cited before page numbers have been issued, to do this please use: J. Li, X. Liu, X. Piao, Z. Sun and L. Pan, *RSC Adv.*, 2015, DOI: 10.1039/C4RA16777E.

ROYAL SOCIETY OF CHEMISTRY

www.rsc.org/advances

Cite this: DOI: 10.1039/c0xx00000x

www.rsc.org/xxxxxx

View Article Online
DOI: 10.1039/C4RA16777E

ARTICLE TYPE

Novel carbon sphere@Bi_2MoO_6 core-shell structure for efficient visible light photocatalysis

Jinliang Li,[a] Xinjuan Liu*[b], Xianqing Piao,[a] Zhuo Sun[a] and Likun Pan,*[a]

Received (in XXX, XXX) Xth XXXXXXXXX 20XX, Accepted Xth XXXXXXXXX 20XX

DOI: 10.1039/b000000x

Carbon sphere (CS) @Bi_2MoO_6 core-shell structure (CS@BMO) composites were successfully synthesized via a solvothermal reaction of CSs and Bi_2MoO_6 precursor in the mixed solution of ethylene glycol and ethanol. The morphology, structure and photocatalytic performance of the composites in the degradation of Rhodamine B (RhB) were characterized by scanning electron microscopy, X-ray diffraction, UV-vis absorption spectroscopy, electrochemical impedance spectra and nitrogen adsorption-desorption, respectively. The results show that the CS@BMO composites exhibit enhanced photocatalytic performance for degradation of RhB with a maximum degradation rate of 95% under visible light irradiation compared with the pure Bi_2MoO_6. The improved photocatalytic performance is ascribed to the enhanced specific surface area and light absorption as well as the reduced electron-hole pair recombination with the presence of CSs in the composites.

1. Introduction

It is well known that TiO_2, ZnO, ZnS and other similar kinds of semiconductor materials with wide band gap have been widely used for clean energy and environmental protection.[1-6] Unfortunately, these materials can only exhibit high photocatalytic activity under ultraviolet light irradiation, which significantly limits their practical applications.[7-9] In order to extend the light response to visible light range for the efficient utilization of sunlight, a variety of visible-light-driven photocatalysts have been developed.[10-13] Recently, Aurivillius oxide semiconductors with general formula $Bi_2A_{n-1}B_nO_{3n+3}$(A=Ca, Sr, Ba, Pb, Na and B=Ti, Nb, Ta, Mo, W), are evoking much interest due to their layered structure and unique properties.[14-17] In particular, Bi_2MoO_6 as a typical Aurivillius oxide, with a narrow band gap of 2.66 eV has a strong absorption in the visible spectrum region. Therefore, it has been exploited for water splitting and degradation of organic contaminants.[18-20] Tian et al.[21] reported Bi_2MoO_6 hollow spheres through solvothermal method and Sun et al.[22] synthesized Bi_2MO_6 nanofibers using electrospinning method, and both of them showed good photocatalytic performance for degradation of Rhodamine B (RhB). However, the quick recombination of photo-generated charge carriers still exists in Bi_2MoO_6, which restrains its photocatalytic performance.[23]

In order to solve this issue, carbon materials, such as carbon nanofibers (CNFs), reduced graphene oxide (RGO) and C_{60}, have been reported as hybrid components to be incorporated into Bi_2MoO_6 due to their low cost, superior chemical stability, and good conductivity.[23-25] Zhang et al.[24] synthesized Bi_2MoO_6 on CNFs by hydrothermal method and found that the composite exhibited an enhanced visible photocatalytic performance for degradation of RhB. Zhao et al.[25] and Zhang et al.[23] prepared C_{60} modified Bi_2MoO_6 and Bi_2MoO_6-RGO composites, respectively, and both of them exhibited much higher photocatalytic activity than pristine Bi_2MoO_6 under visible light irradiation. These carbon materials act as excellent electron-acceptor/transport materials in the process of photocatalysis to effectively facilitate the migration of photoinduced electrons and to hinder the charge recombination in electron-transfer processes, which enhances the photocatalytic performance of Bi_2MoO_6. Similarly, carbon spheres (CSs) have attracted much interest for wide application in supercapacitors, rechargeable battery and capacitive deionization due to their excellent electronic properties, superior chemical stability and high specific surface area,[26-31] and they have also been used for photocatalysis as electron-acceptor/transport material in composites.[31] Unfortunately, little attention has been focused on the synthesis and photocatalytic application of CS-Bi_2MoO_6 composite by now.

In this work, CS@Bi_2MoO_6 core-shell structure (CS@BMO) composites were synthesized through solvothermal reaction of CSs and Bi_2MoO_6 precursor in an ethylene glycol (EG)/ethanol mixed solution, and their photocatalytic performance for degradation of RhB was investigated. Compared with direct mixture of CSs and Bi_2MoO_6 (CS-BMO), the core-shell structure offers more efficient photoinduced charge separation which can enhance the photocatalytic activity.[32-34] Therefore, the CS@BMO composites exhibit enhanced photocatalytic performance compared with pure Bi_2MoO_6 and CS-BMO.

2. Experimental

2.1 Synthesis

CSs were obtained by a hydrothermal method. In a typical synthesis, 8.917 g glucose ($C_6H_{12}O_6.H_2O$) was dissolved in 60 mL deionized (DI) water. Subsequently, the glucose solution was transferred into a 100 mL teflon-lined stainless steel autoclave, which was heated to 180 °C for 12 h. Then the obtained sample was isolated by washing five times with DI water, dried in a

vacuum oven at 80 °C for 24 h, and then annealed at 1000 °C in nitrogen atmosphere for 1 h. The obtained CSs were put into an 80°C solution of concentrated nitric acid and sulfuric acid (1:2 in volume) and kept for 5 h. The mixture was cooled by ice-water bath and diluted with DI water. Finally, the CSs were isolated by washing five times with distilled water, dried in a vacuum oven at 60 °C for 24 h.

The CS@BMO composites were obtained by a solvothermal reaction. In a typical case, 0.3638 g $Bi(NO_3)_3$•$5H_2O$ and 0.0908 g Na_2MoO_4•$2H_2O$ were dissolved in 7.5 mL of EG under magnetic stirring, respectively. The two solutions were mixed together, and then different amount of CSs were added into the mixed solution. Subsequently, 45 mL ethanol was slowly added into the above solution, followed by stirring for 20 min. The resulting clear solution was transferred into a 100 mL teflon-lined stainless steel autoclave, which was heated to 160 °C for 12 h. The obtained sample was isolated by washing five times with DI water, dried in a vacuum oven at 80 °C for 24 h, and then annealed at 350 °C in air atmosphere for 1 h. The samples synthesized using 2 wt%, 5 wt% and 7 wt% CSs, were named as CS@BMO-2, CS@BMO-5, and CS@BMO-7. Pure Bi_2MoO_6 was synthesized by a direct solvothermal reaction of the Bi_2MoO_6 precursor solution for comparison. CS-BMO was also prepared by directly mixing Bi_2MoO_6 with 5 wt% CSs. For the electrochemical impedance spectra (EIS) testing, 90 mg sample with 0.2 mL 2.5 wt% polyvinyl alcohol binder was homogenously mixed in water to form slurry. Then, the resultant slurries were coated on the graphite flake (2 cm×2 cm). Finally, these prepared electrodes were dried in a vacuum oven at 60 °C for 24 h.

2.2 Characterization

The surface morphology, structure and composition of the samples were characterized by field-emission scanning electron microscopy (FESEM, Hitachi S-4800), X-ray diffraction (XRD, Holland Panalytical PRO PW3040/60) with Cu-Kα radiation (V =30 kV, I = 25 mA), and energy dispersive X-ray spectroscopy (EDS, JEM-2100). The diffuse absorption spectra of the samples were recorded on a UV-vis spectrophotometer (Hitachi U-3900) equipped with an integrated sphere attachment. The Brunauer-Emmett-Teller (BET) specific surface areas of the samples were evaluated on the basis of nitrogen adsorption isotherms measured at 77 K using a BELSORP-max nitrogen adsorption apparatus (Micrometitics, Norcross, GA). EIS measurement was carried out on an electrochemical workstation (AUTOLAB PGSTAT302N) under dark condition using a three electrode configuration with a Pt foil as counter electrode and a standard calomel electrode as reference electrode. The electrolyte was 10 mg L^{-1} RhB aqueous solution. EIS were recorded in the frequency range of 0.1 Hz-1 MHz, and the applied bias voltage and ac amplitude were set at open-circuit voltage and 10 mV.

2.3 Photocatalytic experiments

The photocatalytic performance of the samples was evaluated through a photochemical reactor (Bilon Co., Ltd). The distance between metal halogen lamp (400 W) and quartz tube is 60 mm, and the filter size (λ > 400 nm) is 30 mm×100 mm. The samples (80 mg) were dispersed in 80 mL RhB aqueous solutions (10 mg L^{-1}). The mixed suspensions were first magnetically stirred in the dark for 30 min to reach the adsorption-desorption equilibrium. Under ambient conditions and stirring, the mixed suspension was exposed to the visible irradiation. At certain time intervals, 2 mL of the mixed suspensions were extracted and centrifuged to remove the photocatalysts. The filtrates were analysed by recording the UV-vis spectra of RhB using Hitachi U-3900 UV-vis spectrophotometer.

3. Results and discussion

Fig. 1(a) shows the FESEM image of CSs. It can be clearly observed that the CSs show uniformly-sized nanospheres with an average diameter of 400 nm. Fig. 1(b) and (c) display the FESEM images of Bi_2MoO_6 and CS@BMO-5. The morphologies of CS@BMO-2 and CS@BMO-7 (not shown here) are similar to that of CS@BMO-5. It is clearly observed that Bi_2MoO_6 shows a yolk-shell structure with closely packed nanosheets on the surface of microspheres by self-assembling. With the addition of CSs in Bi_2MoO_6 precursor, the Bi_2MoO_6 begins growing on the surface of CSs, as shown in Fig. 1(c). From the enlarged image of CS@BMO-5 in Fig. 1(d), the hierarchically structured outer spherical shell can be observed which consists of ultrathin nanosheets, and the inner core is composed of CSs. The C elemental mapping image corresponding to Fig. 1(c) is shown in Fig. 1(e). It can be observed that the C element is distributed in Bi_2MoO_6, which indicates that the CSs are coated by Bi_2MoO_6 in the composite. The CS@BMO-5 is further identified by EDS linked to FESEM (Fig. 1(f)). The peaks of Bi, Mo and O are found in EDS. The atom ratio of Bi and Mo is 2:1, indicating the existence of Bi_2MoO_6 in the composite.

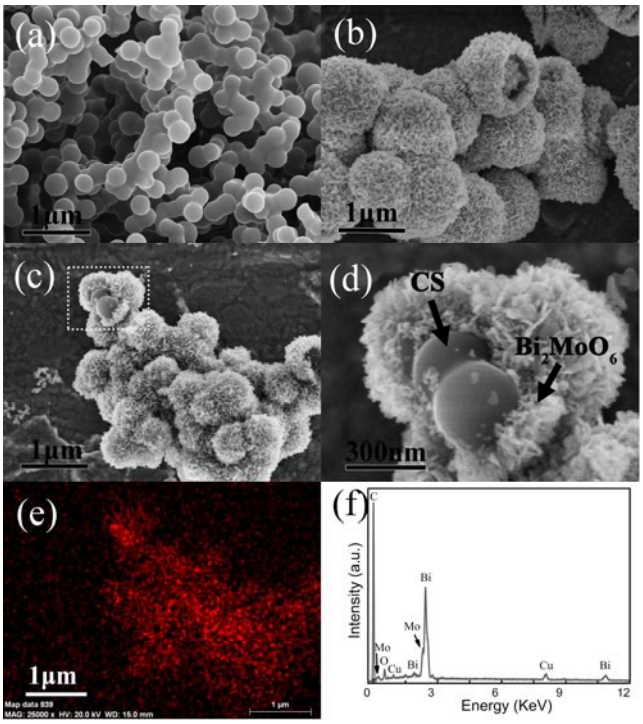

Fig. 1 FESEM images of (a) CSs, (b) Bi_2MoO_6 and (c) CS@BMO-5; (d) enlarged FESEM image of CS@BMO-5; (e) C elemental mapping image and (f) EDS of CS@BMO-5.

It is well known that the CSs could be electronegative after acid treatment,[35-37] and the $[Bi_2O_2]^{2+}$ and $[MoO_4]^{2-}$ were co-

coordinated to be complex compounds with the EG.[21, 38] The possible growth mechanism of CS@BMO composites is proposed, as shown in Fig. 2. The surface of CSs becomes electronegative after acid treatment. As the primary growth unit of Bi_2MoO_6 in solvothermal reaction, $[Bi_2O_2]^{2+}$ with positive charges can be easily absorbed on the surface of CSs with negative charges due to the electrostatic interaction to form Bi_2MoO_6 nuclei.[35] The Bi_2MoO_6 nuclei gradually grow up to form Bi_2MoO_6 nanosheets during the solvothermal process. Finally the Bi_2MoO_6 nanosheets were coated on the surface of CSs to form CS@BMO composite.

Fig. 2 Schematic illustration of the growth process of CS@BMO composite.

Fig. 3 shows the XRD patterns of CSs, Bi_2MoO_6, CS@BMO-2, CS@BMO-5 and CS@BMO-7. The CSs exhibit a (002) diffraction peak at 26° and a (100) peak at 44.5°.[28] The XRD analysis shows that the main diffraction peaks of Bi_2MoO_6 and CS@BMO composites correspond to those of orthorhombic phase Bi_2MoO_6 (JCPDS 21-0102), which demonstrates that the presence of CSs does not result in the development of new crystal orientations of Bi_2MoO_6.[39, 40] No typical diffraction peaks of carbon species are observed in the composites, which may be due to the low amount of CSs.

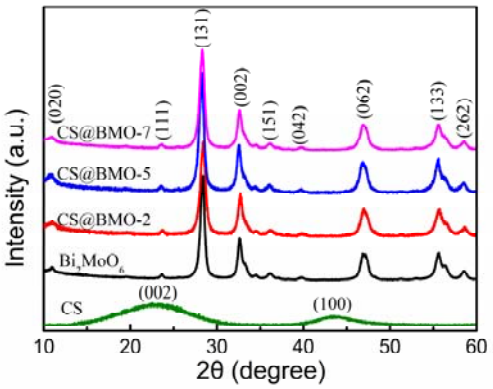

Fig. 3 XRD patterns of CSs, Bi_2MoO_6, CS@BMO-2, CS@BMO-5 and CS@BMO-7.

The UV-vis diffuse absorption spectra of Bi_2MoO_6, CS@BMO-2, CS@BMO-5 and CS@BMO-7 are shown in Fig. 4. For all the samples, a significant absorption at the wavelength of less than 460 nm can be ascribed to the band gap of Bi_2MoO_6 (≈ 2.66 eV).[41] A comparison of the absorption spectra between the Bi_2MoO_6 and CS@BMO shows that the latter exhibits a broad absorption in the visible-light region. This is attributed to the presence of CSs in the CS@BMO composites, and such a broad absorption increases with the increase of CSs content, corresponding to a color change of the composites from yellow to gray, as shown in Fig. 5. A further observation indicates that all the CS@BMO composites show almost the same absorption edge as that of pure Bi_2MoO_6, implying that carbon is not incorporated into the lattice of Bi_2MoO_6 to modify its band gap.

View Article Online
DOI: 10.1039/C4RA16777E

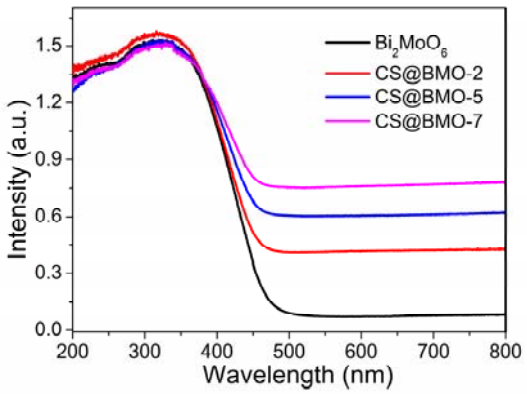

Fig. 4 UV-vis diffuse absorption spectra of Bi_2MoO_6, CS@BMO-2, CS@BMO-5 and CS@BMO-7.

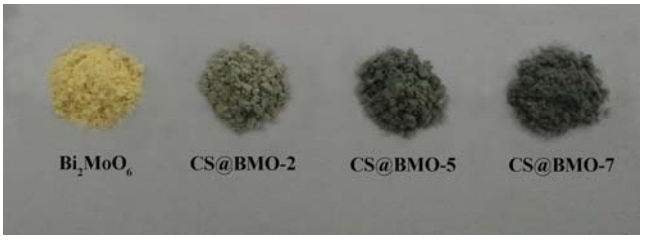

Fig. 5 Photographs of Bi_2MoO_6, CS@BMO-2, CS@BMO-5 and CS@BMO-7.

The charge transfer and recombination behaviours of the samples were studied by analysing the EIS under dark condition. Fig. 6 shows the typical Nyquist plots of Bi_2MoO_6, CS@BMO-2, CS@BMO-5 and CS@BMO-7. The semicircle is ascribed to the contribution of the charge transfer resistance (R_{ct}) and constant phase element (CPE) at the photocatalyst/electrolyte interface. The inclined line, resulted from the Warburg impedance (Z_W), corresponds to the ion diffusion process in the electrolyte.[42, 43] The corresponding equivalent circuit is shown in the inset of Fig. 6. It can be observed that the R_{ct} decreases with the increase of CSs content. It indicates that the introduction of CSs in Bi_2MoO_6 favors the electron transfer and suppresses the charge recombination in Bi_2MoO_6, which is beneficial to the photocatalytic performance. However, when the CSs content is further increased (CS@BMO-7), the R_{ct} increases, which is possibly because excessive CSs in the composite acts as recombination centre instead of providing an election pathway and promotes the recombination of electron-hole pairs in CSs.

Nitrogen adsorption-desorption isotherms and pore size distribution curves (inset) of Bi_2MoO_6 and CS@BMO-5 are displayed in Fig. 7. It can be seen that both of the samples show type IV isotherms with H_3 hysteresis loops.[44, 45] This behavior

may be caused by the existence of non-rigid aggregates.[46] The specific surface areas of Bi_2MoO_6 and CS@BMO-5 are 27.53 m^2 g^{-1} and 58.88 m^2 g^{-1}, respectively, which means that the CSs are helpful to increase the specific surface area of the composite. The pore size distribution curves of Bi_2MoO_6 and CS@BMO-5 show that the samples mainly consist of mesopores. Compared with the Bi_2MoO_6, the CS@BMO-5 shows more mesopores, which can supply more surface active sites and is beneficial to the photocatalytic performance.[47]

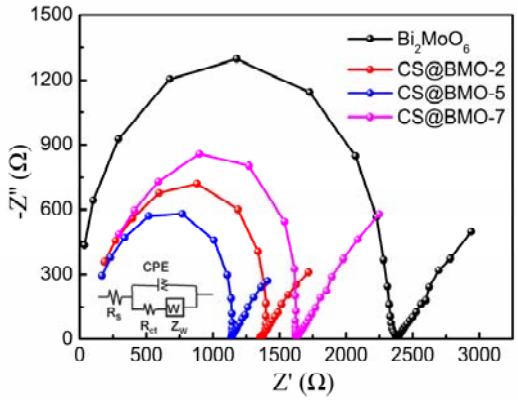

Fig. 6 Nyquist plots of Bi_2MoO_6, CS@BMO-2, CS@BMO-5 and CS@BMO-7. Inset is the corresponding equivalent circuit model.

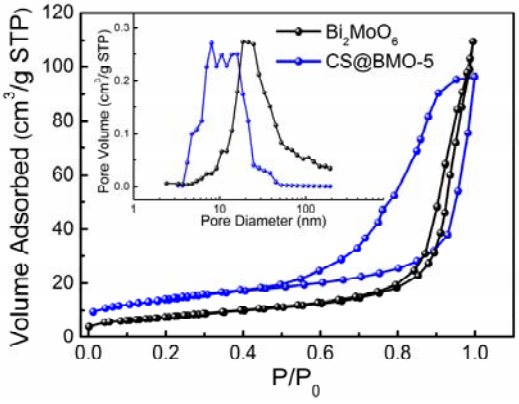

Fig. 7 Nitrogen adsorption-desorption isotherms and corresponding pore size distribution curves (inset) of Bi_2MoO_6 and CS@BMO-5.

Photocatalytic degradation of RhB by Bi_2MoO_6, CS@BMO-2, CS@BMO-5 and CS@BMO-7 was performed under visible light irradiation, as shown in Fig. 8. The normalized temporal concentration changes (C/C_0) of RhB during the photocatalytic process are proportional to the normalized maximum absorbance (A/A_0), which can be derived from the change in the RhB absorption profile at a given time interval. The corresponding adsorption experiments before photocatalysis were shown in Fig. S1 (EIS†), and the results indicate that the adsorption of RhB is increased with the increase of the content of CSs in the composites, which is beneficial to the photocatalytic process.[48] From Fig. 8, it is observed that the concentration of RhB is almost not changed under visible light irradiation in the absence of the photocatalyst. The CS@BMO composites exhibit better photocatalytic performance than pure Bi_2MoO_6 and the photocatalytic performance is dependent on the proportion of CSs in the composites. The degradation rate of RhB for Bi_2MoO_6 is 60%. When CSs is introduced into Bi_2MoO_6, the degradation rate is increased to 72% for CS@BMO-2, and reaches a maximum value of 95% for CS@BMO-5. The enhancement of the photocatalytic performance should be mainly ascribed to the reduction in electron-hole pair recombination due to the stepwise structure of energy levels constructed in CS@BMO composite, as shown in Fig. 9. The conduction band (CB) and valence band (VB) of Bi_2MoO_6 is -0.32 V and 2.34 V (vs. NHE), respectively. The work function of CS is about -0.1 V (vs. NHE).[49] Such energy levels are beneficial for photo-induced electrons to transfer from the CB of Bi_2MoO_6 to the CSs, which can efficiently separate the photo-induced electrons and holes and hinder the charge recombination in electron-transfer process, as indicated by EIS measurement. The holes oxidize the adsorbed H_2O molecules to •OH radicals, which acts the oxidant in photocatalytic reactions. Furthermore, the increases in the light absorption and specific surface area with the presence of CSs are also the important reasons for the enhanced photocatalytic performance of the CS@BMO composites, which has been confirmed by UV-vis absorption spectra and nitrogen adsorption-desorption isotherms.[50-52] However, when the CSs content is further increased, the degradation rate is decreased to 85% for CS@BMO-7, which may be due to the increased recombination of photo-generated electron-hole pairs in excessive CSs. As a contrast experiment, the photocatalytic performance of the CS-BMO was measured, and the degradation rate is only 66%, which is inferior to those for the CS@BMO composites. The reason should be ascribed the more efficient close contact between the CSs and Bi_2MoO_6 in the core-shell structure, which is helpful to the electron transfer in the composites.[53, 54]

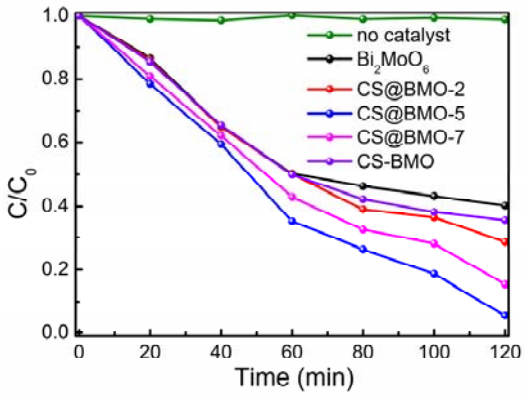

Fig. 8 Photocatalytic degradation of RhB by Bi_2MoO_6, CS@BMO-2, CS@BMO-5, CS@BMO-7 and CS-BMO under visible light irradiation.

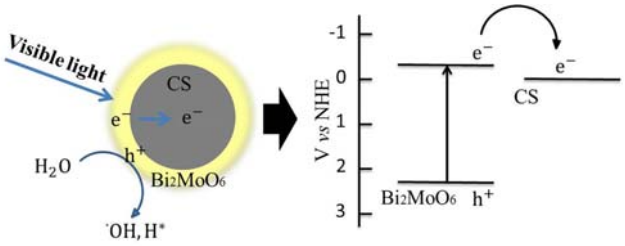

Fig. 9 Schematic diagram of energy levels of Bi_2MoO_6 and CS

4. Conclusions

CS@BMO composites were successfully synthesized via solvothermal method and their photocatalytic performances were investigated. The results show that (i) CS@BMO composites exhibit better photocatalytic performance than Bi_2MoO_6, and their photocatalytic performance is related to the CSs content in the composites; (ii) CS@BMO-5 achieves a highest RhB degradation rate of 95% at 120 min; (iii) the enhanced photocatalytic performance is ascribed to the increased light adsorption, the reduced electron-hole pair recombination and the larger specific surface area with the presence of CSs in the composites.

Acknowledgements

Financial support from the National Natural Science Foundation of China (No. 21401180 and 51102095) and Research Fund for the Doctoral Program of Higher Education of China (No. 20110076120023) are gratefully acknowledged.

Notes and references

[a]*Engineering Research Center for Nanophotonics & Advanced Instrument, Ministry of Education, Shanghai Key Laboratory of Magnetic Resonance, Department of Physics, Department of Physics, East China Normal University, Shanghai 200062 China, Fax: +86 21 62234321; Tel: +86 21 62234132; E-mail: lkpan@phy.ecnu.edu.cn*

[b]*Institute of Coordination Bond Metrology and Engineering, College of Materials Science and Engineering, China Jiliang University, Hangzhou 310018, China; E-mail: lxj669635@126.com*

1. T. Kamegawa, S. Matsuura, H. Seto and H. Yamashita, *Angew. Chem. Int. Ed.*, 2013, **52**, 916-919.
2. M. Murdoch, G. Waterhouse, M. Nadeem, J. Metson, M. Keane, R. Howe, J. Llorca and H. Idriss, *Nat. Chem.*, 2011, **3**, 489-492.
3. Y. Lv, C. Pan, X. Ma, R. Zong, X. Bai and Y. Zhu, *Appl. Catal. B: Environ.*, 2013, **138–139**, 26-32.
4. Y. Wang, R. Shi, J. Lin and Y. Zhu, *Energy Environ. Sci.*, 2011, **4**, 2922-2929.
5. J. Zhang, S. Liu, J. Yu and M. Jaroniec, *J. Mater. Chem.*, 2011, **21**, 14655-14662.
6. X. J. Liu, X. J. Wang, H. L. Li, L. K. Pan, T. Lv, Z. Sun and C. Q. Sun, *J. Mater. Chem.*, 2012, **22**, 16293-16298.
7. R. Liu, P. Wang, X. Wang, H. Yu and J. Yu, *J. Phys. Chem. C*, 2012, **116**, 17721-17728.
8. X. J. Liu, L. K. Pan, Q. F. Zhao, T. Lv, G. Zhu, T. Q. Chen, T. Lu, Z. Sun and C. Q. Sun, *Chem. Eng. J.*, 2012, **183**, 238-243.
9. M. Sharma, T. Jain, S. Singh and O. Pandey, *Sol. Energy*, 2012, **86**, 626-633.
10. Y. Liu, L. Yu, Y. Hu, C. Guo, F. Zhang and X. W. D. Lou, *Nanoscale*, 2012, **4**, 183-187.
11. F. A. Frame and F. E. Osterloh, *J. Phys. Chem. C*, 2010, **114**, 10628-10633.
12. Y. Wang, Z. Wang, S. Muhammad and J. He, *CrystEngComm*, 2012, **14**, 5065-5070.
13. L. K. Pan, X. J. Liu, Z. Sun and C. Q. Sun, *J. Mater. Chem. A*, 2013, **1**, 8299-8326.
14. Y. Liu, M. Zhang, L. Li and X. Zhang, *Appl. Catal. B: Environ.*, 2014, **160–161**, 757-766.
15. X. C. Song, Y. F. Zheng, R. Ma, Y. Y. Zhang and H. Y. Yin, *J. Hazard. Mater.*, 2011, **192**, 186-191.
16. Y. Xu and W. Zhang, *Appl. Catal. B: Environ.*, 2013, **140-141**, 306-316.
17. Y. Wang, W. Wang, H. Mao, Y. Lu, J. Lu, J. Huang, Z. Ye and B. Lu, *ACS Appl. Mater. Interf.*, 2014, **6**, 12698-12706.
18. J. L. Li, X. J. Liu, L. K. Pan, W. Qin and Z. Sun, *RSC Adv.*, 2014, **4**, 62387-62392.
19. C. Guo, J. Xu, S. Wang, L. Li, Y. Zhang and X. Li, *CrystEngComm*, 2012, **14**, 3602-3608.
20. Z. Li, X. Chen and Z. Xue, *CrystEngComm*, 2013, **15**, 498-508.
21. G. Tian, Y. Chen, W. Zhou, K. Pan, Y. Dong, C. Tian and H. Fu, *J. Mater. Chem.*, 2011, **21**, 887-892.
22. Y. Sun, W. Wang, S. Sun and L. Zhang, *CrystEngComm*, 2013, **15**, 7959-7964.
23. Y. Zhang, Y. Zhu, J. Yu, D. Yang, T. W. Ng, P. K. Wong and J. Yu, *Nanoscale*, 2013, **5**, 6307-6310.
24. M. Zhang, C. Shao, J. Mu, X. Huang, Z. Zhang, Z. Guo, P. Zhang and Y. Liu, *J. Mater. Chem.*, 2012, **22**, 577-584.
25. X. Zhao, H. Liu, Y. Shen and J. Qu, *Appl. Catal. B: Environ*, 2011, **106**, 63-68.
26. N. P. Wickramaratne, J. Xu, M. Wang, L. Zhu, L. Dai and M. Jaroniec, *Chem. Mater.*, 2014, **26**, 2820-2828.
27. A. D. Roberts, X. Li and H. Zhang, *Chem. Soc. Rev.*, 2014, **43**, 4341-4356.
28. T. Q. Chen, L. K. Pan, T. Lu, C. L. Fu, D. H. Chua and Z. Sun, *J. Mater. Chem. A*, 2014, **2**, 1263-1267.
29. Y. Liu, L. K. Pan, T. Q. Chen, X. T. Xu, T. Lu, Z. Sun and D. H. Chua, *Electrochim. Acta*, 2015, **151**, 489-496.
30. K. Zhang, Q. Zhao, Z. Tao and J. Chen, *Nano Res.*, 2013, **6**, 38-46.
31. W. Zhao, Y. Wang, Y. Yang, J. Tang and Y. Yang, *Appl. Catal. B: Environ*, 2012, **115-116**, 90-99.
32. C. Kuo, Y. Yang, S. Gwo and M. H. Huang, *J. Am. Chem. Soc.*, 2010, **133**, 1052-1057.
33. W. Chen, T. Yang and Y. Hsu, *Chem. Mater.*, 2008, **20**, 7204-7206.
34. P. V. Kamat, *J. Phys. Chem. C*, 2008, **112**, 18737-18753.
35. Z. Jiang, B. Huang, Z. Lou, Z. Wang, X. Meng, Y. Liu, X. Qin, X. Zhang and Y. Dai, *Dalton Trans.*, 2014, **43**, 8170-8173.
36. H. ShamsiJazeyi and T. Kaghazchi, *J. Ind. Eng. Chem.*, 2010, **16**, 852-858.
37. F. Meng, J. Zhao, Y. Ye, X. Zhang and Q. Li, *Nanoscale*, 2012, **4**, 7464-7468.
38. Y. Miao, G. Pan, Y. Huo and H. Li, *Dyes Pigments*, 2013, **99**, 382-389.
39. D. Yue, D. Chen, Z. Wang, H. Ding, R. Zong and Y. Zhu, *Phys. Chem. Chem. Phys.*, 2014, **16**, 26314-26321.
40. H. Li, J. Liu, W. Hou, N. Du, R. Zhang and X. Tao, *Appl. Catal. B: Environ.*, 2014, **160–161**, 89-97.
41. Z. Zhang, W. Wang, D. Jiang and J. Xu, *Catal. Comm.*, 2014, **55**, 15-18.
42. J. L. Li, X. J. Liu, L. K. Pan, W. Qin, T. Q. Chen and Z. Sun, *RSC Adv.*, 2014, **4**, 9647-9651.
43. W. Qin, T. Q. Chen, L. K. Pan, L. Y. Niu, B. W. Hu, D. S. Li, J. L. Li and Z. Sun, *Electrochim. Acta*, 2015, **153**, 55-61.
44. J. A. Foster, D. W. Johnson, M. O. M. Pipenbrock and J. W. Steed, *New J. Chem.*, 2014, **38**, 927-932.
45. Y. H. Tan, J. A. Davis, K. Fujikawa, N. V. Ganesh, A. V. Demchenko and K. J. Stine, *J. Mater. Chem.*, 2012, **22**, 6733-6745.
46. C. Belver, P. Aranda and E. Ruiz Hitzky, *J. Mater. Chem. A*, 2013, **1**, 7477-7487.
47. X. J. Liu, L. K. Pan, T. Lv, G. Zhu, Z. Sun and C. Q. Sun, *Chem. Commun.*, 2011, **47**, 11984-11986.
48. Y. Zhang, Z. R. Tang, X. Fu and Y. J. Xu, *ACS Nano*, 2010, **4**, 7303-7314.
49. P. Zhang, C. Shao, Z. Zhang, M. Zhang, J. Mu, Z. Guo and Y. Liu, *Nanoscale*, 2011, **3**, 3357-3363.
50. X. Liu, H. Cao and J. Yin, *Nano Res.*, 2011, **4**, 470-482.
51. S. Sajjad, S. A. K. Leghari, F. Chen and J. Zhang, *Chem. Eur. J.*, 2010, **16**, 13795-13804.
52. X. Zhang, X. Lu, Y. Shen, J. Han, L. Yuan, L. Gong, Z. Xu, X. Bai, M. Wei, Y. Tong, Y. Gao, J. Chen, J. Zhou and Z. L. Wang, *Chem. Commun.*, 2011, **47**, 5804-5806.
53. Y. P. Xie, Z. B. Yu, G. Liu, X. L. Ma and H. Cheng, *Energy Environ. Sci.*, 2014, **7**, 1895-1901.
54. N. Zhang, S. Liu and Y. Xu, *Nanoscale*, 2012, **4**, 2227-2238.

View Article Online DOI: 10.1039/C4RA16777E